Dynamics of a Glassy Polymer Nanocomposite during Active Deformation

Robert A. Riggleman,[†] Gregory N. Toepperwein,[‡] George J. Papakonstantopoulos,[§] and Juan J. de Pablo*,[‡]

Department of Chemical Engineering; University of California, Santa Barbara, California 93106; Department of Chemical and Biological Engineering, University of Wisconsin, Madison, Wisconsin 53706; and Analytical and Systems Division, Arkema Inc. R&D Center, King of Prussia, Pennsylvania 19406

Received December 26, 2008; Revised Manuscript Received March 26, 2009

ABSTRACT: We have examined the response of a polymer and a polymer nanocomposite glass to creep and constant strain rate deformations using Monte Carlo and molecular dynamics simulations. We find that nanoparticles stiffen the polymer glass, as evidenced by an increase in the initial slope of the stress−strain curve and a suppression of the creep response. In contrast to previous reports, we also find that, during deformation, the effective relaxation time or mobility of the material is only qualitatively characterized by the instantaneous strain rate. Constant strain rate and constant stress deformations have different effects on the material's position on its energy landscape, and neither a mechanical variable, such as the stress or strain rate, nor a thermodynamic variable, such as the material's position on its energy lanscape, is uniquely indicative of the relaxation times in the material.

1. Introduction

Nanoparticle reinforced polymeric materials, or nanocomposites, have received a considerable amount of attention[1−8] in recent years. A wide array of properties can be altered through the addition of nanoparticles. Some authors have reported increases[1,8] or decreases[2] the plateau modulus, depending on the interactions between the nanoparticles and the polymer matrix. Nanoparticles have also been reported to toughen the polymer.[7] However, because of the difficulties associated with dispersing nanoparticles in a polymer matrix, experimental results have been difficult to interpret.

Applications of polymer nanocomposites, for example in the automotive and aviation industries, often require these materials to exist in a glassy state. Furthermore, the glassy composite is generally subjected to applied stresses and repeated cycles of deformation. It is therefore of interest to understand at a fundamental level how such materials respond to the effects of deformation. Recent experimental,[9,10] theoretical,[11] and computational studies[12,13] have shown that plastic deformation can lead to significant changes in the segmental dynamics of polymer glasses. For example, during a creep experiment on lightly cross-linked poly(methyl methacrylate) (PMMA), Lee et al. found that the relaxation time can be up to 1000 smaller than in the undeformed sample.

Several simulation studies have examined the effects of deformation on the dynamics of both small-molecule glasses[14−20] and low molecular weight polymers.[21−24] Some key results obtained from molecular simulations of low molecular weight materials include a demonstration of shear-induced melting of the binary Lennard-Jones glass[18] and direct observation that deformation can reduce the energy barriers that separate inherent structures on the potential energy landscape (PEL).[14,15]

In previous work, we have employed molecular simulations of a polymer glass and demonstrated that nonequilibrium molecular dynamics simulations of a polymer glass undergoing creep can capture the effects of deformation observed in experiments: the segmental relaxation times are enhanced by over 2 orders of magnitude, depending on the value of the applied stress, the relaxation times are not constant during a creep deformation, and the dynamics are strongly correlated with the instantaneous strain rate experienced by the material.[12] By applying both tensile and compressive deformations, it was shown that changes in the free volume cannot explain the observed changes in dynamic properties. A more promising approach appears to be the PEL view of glassy dynamics,[13] an idea that is further explored in this article.

The property changes experienced by amorphous polymeric glasses under deformation remain poorly understood. In the absence of detailed molecular-level observations of mobility during deformation, the framework for analysis of deformation-induced mobility has remained that presented by Eyring in 1936.[25] In Eyring's model, a deformation lowers the energy barriers that inhibit mobility in the material. While capable of describing the effects of constant stress deformations on changes in the relaxation time, several aspects of the Eyring model have been challenged by recent experimental observations and results from simulations. The Eyring model postulates that an applied stress should only affect dynamics in the direction of the applied stress; our recent work has demonstrated that the dynamics are uniformly enhanced in all directions.[13] The Eyring model does not consider relaxation during postyield flow and strain hardening, and not surprisingly, it fails to describe the dynamics during those regimes.[26] More recent work by Chen and Schweizer[11,27] postulates that the stress behaves as an isotropic work term that reduces the energy barriers for relaxation in all directions, an idea that is in good agreement with earlier simulations.[13]

An additional challenge associated with deformation-induced mobility pertains to our limited of understanding of the origins of strain hardening. Recent simulations and experiments have provided significant new insights into strain hardening. Hoy and Robbins[28−30] have shown that entropic network theories are unable to capture many of the trends associated with strain hardening, including the temperature and strain rate dependence. They have also broken the stress into entropic and energetic components to show that strain hardening is primarily due to a sharp increase in the energetic contribution to the stress tensor, which arises as chains are pulled tight between entanglements;

* To whom correspondence should be addressed.
[†] University of California.
[‡] University of Wisconsin.
[§] Arkema Inc. R&D Center.

10.1021/ma802865n CCC: $40.75
Published on Web 04/30/2009

the entropic contribution to the stress appears to be much too small to explain strain hardening.[30] Recent work of Chen and Schweizer in which strain hardening is attributed to changes in the dynamics associated with anisotropic chain conformations appears to capture many of the features associated with strain hardening in simulations and experiments.[27]

In recent work we have resorted to a combination of experiments and simulations to establish that the molecular models considered in our computational work provide a faithful description of molecular mobility in polymeric glasses undergoing deformation.[13,26,31] Armed with that model, we extend our previous studies in two key ways. First, we provide a detailed comparison of constant strain rate and constant stress deformations, including the effects of each mode of deformation on the changes in the materials' position on its energy landscape. Second, in this work we examine how the addition of nanoparticles influences the relaxation of a nanocomposite under creep and under constant strain rate deformation. Experimental molecular mobility data are not available for such systems, and we therefore must rely purely on the results of simulations to provide the insights required to build a theory of composites under deformation that goes beyond the ideas originally proposed by Eyring. Our simulations aim to establish the behavior of a standard reference model to which subsequent results can be compared. With that goal in mind, the particles are fully dispersed in the material and their interactions with the polymer are relatively weak. Our simulations suggest that the pure polymer and the nanocomposite exhibit qualitatively similar deformation behaviors. The nanoparticles stiffen the polymer, and a higher stress is required during creep to achieve the same amount of deformation. The dynamics in both systems are up to 1000 times faster during deformation than at rest. A comparison of the results from creep (constant stress) and constant strain rate deformations and their relation to their respective PELs reveal qualitative differences in the dynamical behavior under these two deformation mechanisms. Finally, we briefly discuss the effects of deformation on the dynamic heterogeneity.

2. Methods

2.1. Molecular Model and Sample Preparation. The polymer model considered in this work has been described in detail in other studies;[5,32,33] here we recount the main details for completeness. The polymer chains are modeled as 500 Lennard-Jones (LJ) interaction sites connected by stiff harmonic bonds. The nanoparticles employed in this study were modeled as spherical shells of LJ interaction sites; one LJ site is placed at the center of each nanoparticle, and 49 other LJ sites are connected to this central site with very stiff harmonic bonds with an equilibrium bond length of $2.0\sigma_{PP}$, where σ_{PP} is the LJ σ parameter associated with the polymer monomers. This yields nanoparticles with a surface shell of LJ sites connected to the central LJ site; the interactions between the sites of the nanoparticles and the sites of the polymer monomers are neutral. That is, $\sigma_{PP} = \sigma_{PN} = 1.0$ and $\epsilon_{PP} = \epsilon_{PN} = 1.0$, where σ_{PN} is the LJ σ value associated with the interactions between the polymer monomers and the nanoparticle interaction sites and ϵ_{PP} and ϵ_{PN} are the LJ ϵ parameters for the polymer−polymer interactions and the polymer−nanoparticle interactions. In order to ensure that the nanoparticles remain dispersed throughout our system during the simulation, $\epsilon_{NN} = 0.5$. The units for all quantities reported in this work are normalized by the LJ parameters of the polymer monomers; e.g., $T = k_B T^*/\epsilon_{PP}$ and $P = P^*\sigma_{PP}^3/\epsilon_{PP}$, $t_{LJ} = t^*(m_{PP}\sigma_{PP}^3/\epsilon_{PP})^{1/2}$, where m_{PP} is the mass of a polymer monomer (taken as unity) and the asterisk implies laboratory units.

The relaxation times in entangled polymers span several decades in time, and the longest relaxation times are inaccessible to MD simulations. Thus, great care must be exercised to ensure proper equilibration of our materials. We employ repeated cycles of Monte Carlo (MC) and molecular dynamics (MD) simulations at high temperatures to both equilibrate and generate independent configurations of both systems. The MC component of the equilibration procedure employs connectivity-altering algorithms, such as configurational-bias double bridging,[34,35] which have been shown to lead to a decay of the end-to-end autocorrelation function for polymer chains as long as those employed in this study. The high temperature ($T = 2.0$) MD component of the equilibration procedure is effective for equilibrating the distribution of particles in our polymer matrix. After generating three independent, equilibrated configurations for both the pure polymer and the nanocomposite, each configuration was cooled from $T = 0.8$ to $T = 0.35$ at a rate of 10^{-4} in the NPT ensemble, with $P = 0.3$. The glass transition temperatures for each system are $T_g = 0.406 \pm 0.001$ and 0.412 ± 0.001 for the pure polymer and nanocomposite, respectively. After cooling to $T = 0.35$, each sample was aged for $t = 10000t_{LJ}$ prior to deformation. All of the equilibration routines were performed using an in-house code, while the production deformation calculations were performed using the LAMMPS simulation package.[36] All results below are averaged over three independent configurations, and error bars represent the standard error of the results among the three configurations.

2.2. Deformation Protocols. Results from both constant stress (creep) and constant strain rate deformations are presented below. For the constant stress deformations, we applied tensile stresses in the *xx*-direction while maintaining a constant pressure in the *yy*- and *zz*-directions. Five values of stress were applied to each system; for the pure polymer, stresses of 0.50, 0.55, 0.59, 0.62, and 0.65 were employed, and for the nanocomposite stresses of 0.59, 0.62, 0.65, 0.69, and 0.73 were employed. The values of 0.59, 0.62, and 0.65 are common to both systems, enabling a comparison at a constant stress; the remaining values were chosen to elicit a similar range of strain responses. We adopt the convention where a positive stress indicates a tensile deformation. We have also performed both tensile and compressive deformations at constant (true) strain rate, where the *x*-direction of the simulation box was deformed at a constant rate while maintaining a constant pressure in the *y*- and *z*-directions. The strain rates employed were $\dot{\epsilon} = 10^{-3}$, 10^{-4}, -10^{-3}, and -10^{-4}.

2.3. Dynamic Properties. We measure the dynamics of each system during deformation by measuring the bond autocorrelation function $C_b(t)$ during various time windows of the deformations, where $C_b(t) = \langle P_2[\hat{b}(t)\cdot\hat{b}(0)]\rangle$, P_2 is the second Legendre polynomial, and $\hat{b}(t)$ is a unit vector aligned along bonds of the polymer backbone. The brackets indicate an average over all of the polymer bonds in the system. This function has proven useful in past studies to quantify segmental dynamics,[12,13,37] and relaxation times obtained from $C_b(t)$ in the supercooled state above T_g have been shown to reflect the α-relaxation time.[38]

In order to quantify the changes in dynamics, we fit $C_b(t)$ to a Kohlrausch−Williams−Watts (KWW) stretched exponential

$$C_b(t) = C_0 e^{-(t/\tau)^\beta} \quad (1)$$

where C_0 is a pre-exponential factor, and τ and β are fitting parameters. We then obtain the effective relaxation times, τ_{eff}, as $\tau_{eff} = \tau\Gamma(1/\beta)/\beta$, where $\Gamma(x)$ is the Gamma function. Although the trends observed in τ_{eff} below are consistent with trends observed in the α-relaxation time predicted by various theories[11,25] and experiments,[10] we wish to emphasize that we do not consider τ_{eff} to be a direct estimate of the α-relaxation time because we are unable to measure the complete decay of $C_b(t)$. We interpret τ_{eff} as a relative change in the segmental dynamics during our deformation simulations. Additionally, we have estimated τ_{eff} for undeformed samples by performing long MD calculations with no deformation; the calculation of τ_{eff} for undeformed samples began after the initial aging period. Unless otherwise stated, all measures of $C_b(t)$ were taken in time windows with a total length $t = 2000t_{LJ}$; we have repeated our calculations for both longer and shorter time window sizes, and none of the results below change qualitatively with other time window sizes.

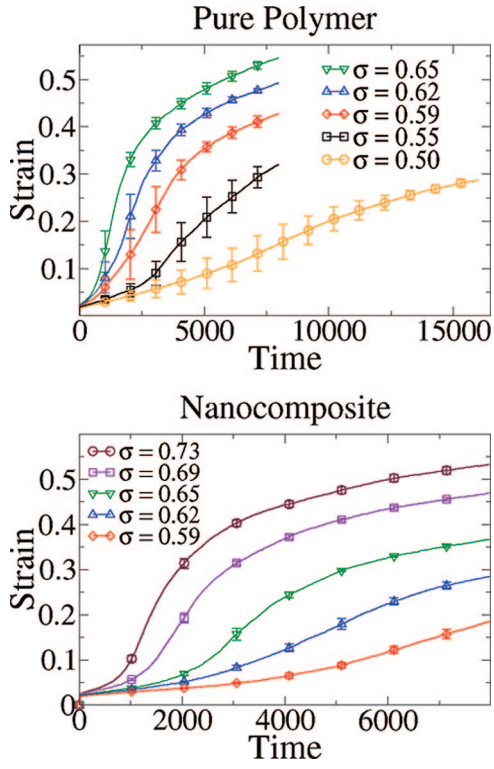

Figure 1. Strain response of the pure polymer and the nanocomposite systems to five different applied stresses. Note that three of the applied stresses ($\sigma = 0.59$, 0.62, and 0.65) were applied to both systems. The two remaining stresses applied to each system were chosen such that a similar range of strain response was observed for both the pure polymer and the nanocomposite.

2.4. Inherent Structure Energy. We characterized our materials' inherent structure energy by sampling configurations every $t = 25t_{LJ}$ and minimizing their potential energy. The minimization algorithm was stopped when the changes in the potential energy were smaller than 10^{-6} or the magnitude of the force vector was smaller than 10^{-8}. The potential energy of the system at this minimum was taken as the inherent structure energy, denoted by U_{IS}. To compare U_{IS} to estimates of τ_{eff} measured in time windows, we then averaged over all of the values of U_{IS} calculated in each time window corresponding to the value of τ_{eff}.

3. Results

3.1. Constant Stress. We begin by presenting the results of the creep deformation of both the pure polymer and the nanocomposite. Five values of stress were applied to both systems, and the strain response is plotted in Figure 1; after application of the tensile stress, there is a rapid elastic response followed by yield where the strain rate begins to increase for both materials (pure and composite). Once the strain reaches $\epsilon \approx 0.20$, the strain rate begins to decrease as strain hardening regime is entered. The nanoparticles stiffen the polymer and suppress the creep response significantly for a given applied stress (e.g., $\sigma = 0.62$). We note that the strain response for the pure polymer differs from that observed in our previous work with a low molecular weight polymer,[13] which indicated much larger deformations for comparable stresses at a slightly higher temperature. This is expected, given that the polymer in this study has a different thermal history and a significantly higher molecular weight, and in this study our materials are subject to a higher pressure.

Figure 2 shows typical $C_b(t)$ curves measured at various points during our deformation simulations for the pure polymer at $\sigma = 0.59$ as well as $C_b(t)$ for the undeformed polymer. The dynamics of the polymer under stress are significantly faster

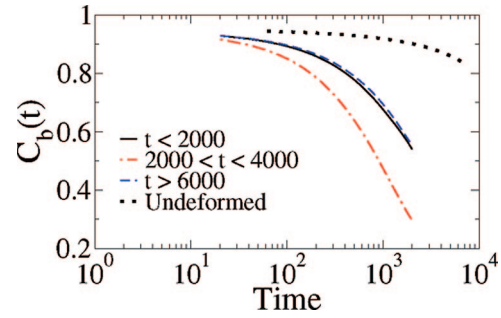

Figure 2. Examples of the bond autocorrelation function, $C_b(t)$, calculated during three different time windows for the pure polymer under a stress of $\sigma = 0.59$. The strain response of the pure polymer at this stress is shown in Figure 1, and the dotted line corresponds to $C_b(t)$ for an undeformed sample.

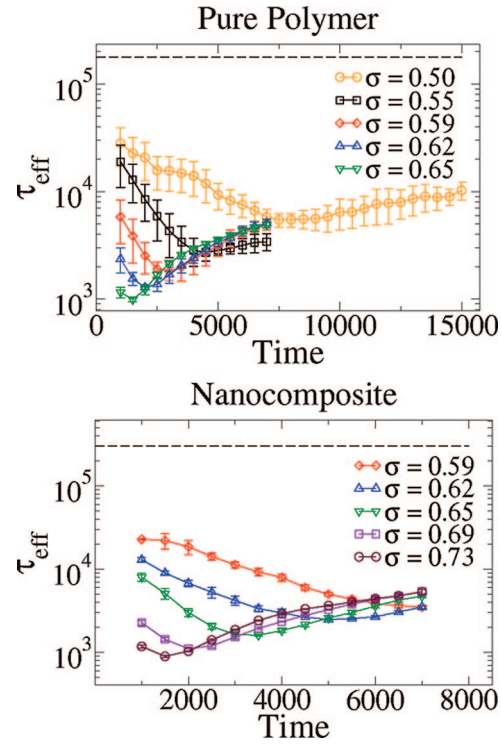

Figure 3. Effective relaxation time, τ_{eff}, as a function of time during creep deformations for the pure polymer and the nanocomposite for each of the five applied stresses. In both cases, the dashed horizontal line corresponds to the estimate of τ_{eff} for an undeformed sample.

than the dynamics of the undeformed sample, as indicated by a faster decay of $C_b(t)$. Additionally, the $C_b(t)$ curve measured during $2000 \leq t \leq 4000$ indicates faster dynamics than the $C_b(t)$ curves for $t \leq 2000$ and $t \geq 6000$. In Figure 1 we see that the strain rate is the highest for the pure polymer when $2000 \leq t \leq 4000$.

Figure 3 shows how τ_{eff} changes with time during the creep deformations. Consistent with experiments[10,26] and our previous results,[13] the dynamics are not constant for a given applied stress, and τ_{eff} appears to be the smallest during periods of high strain rate. For both the pure polymer and the nanocomposite, changes in τ_{eff} larger than 2 orders of magnitude are observed. At a constant stress (e.g., $\sigma = 0.62$), the dynamics are significantly faster in the pure polymer than in the nanocomposite.

Figure 4 plots the inherent structure energy, U_{IS}, against time during our creep deformations for both systems. The behavior in the two systems is qualitatively similar: U_{IS} is not constant

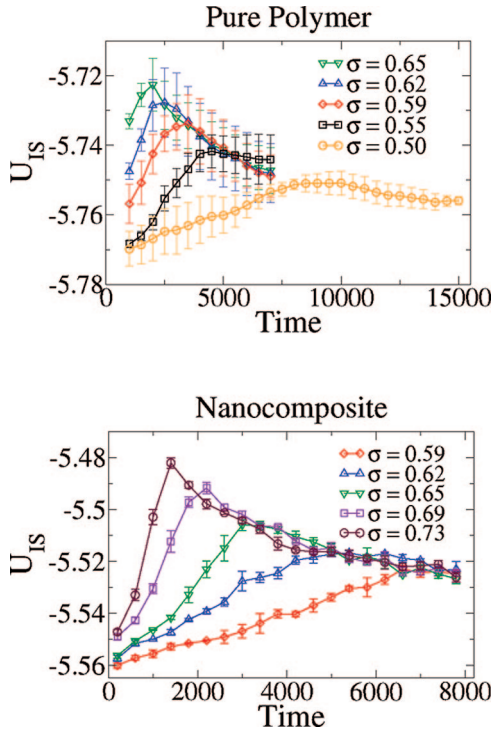

Figure 4. Inherent structure energy, U_{IS}, as a function of time during creep deformations for both systems at each of the five applied stresses.

with time and tends to be highest during periods of high strain rate.

3.2. Constant Strain Rate. Figure 5 shows the stress−strain curves obtained for both the pure polymer and the nanocomposite for both tension and compression at two different strain rates. All curves exhibit similar features: there is an initial elastic response followed by yield and strain softening when the strain $\epsilon \approx 0.05$. Finally, for strains beyond $\epsilon \approx 0.10$ the stress rises again as strain hardening begins. The Young's modulus can be obtained by fitting the linear part of the elastic response ($\epsilon \leq 0.02$ in our case) to $\sigma = E_Y\epsilon$. Under tension, at a true strain rate of 10^{-4}, $E_Y = 20.9 \pm 3.17$ and 29.3 ± 2.0 for the pure polymer and the nanocomposite, respectively. Under compression, at the same strain rate, $E_Y = 30.4 \pm 0.36$ and 33.7 ± 0.54 for the pure polymer and the nanocomposite; both under tension and compression, the nanocomposite system is stiffer, consistent with the suppressed strain response observed in the creep deformations described above.

We measure the dynamics during constant-rate deformations using the time window approach employed above for creep deformations. For our lower strain rate ($\dot{\epsilon} = 10^{-4}$), the time windows have the same length as those employed in creep deformations ($t = 2000t_{LJ}$, which corresponds to a strain of 0.2). We reduce the size of the time windows by 1 order of magnitude for the high strain rate deformations. This is necessary because the total length of the high strain rate deformation simulations is smaller than one time window for the slower strain rate and the creep deformations; we again emphasize that this has no qualitative effect on our results. The results of these calculations are shown in the insets of Figure 6. It is clear from this figure that the dynamics are slower for $\epsilon \leq 0.10$, which is approximately where strain hardening sets in; beyond this point, the dynamics are essentially constant. To further explore the decrease in mobility at small strains, we calculated τ_{eff} using even smaller time windows for $\epsilon \leq 0.05$, and these estimates of τ_{eff} are shown in the main plots of Figure 6. We find that τ_{eff} decreases by over 2 orders of magnitude during the elastic

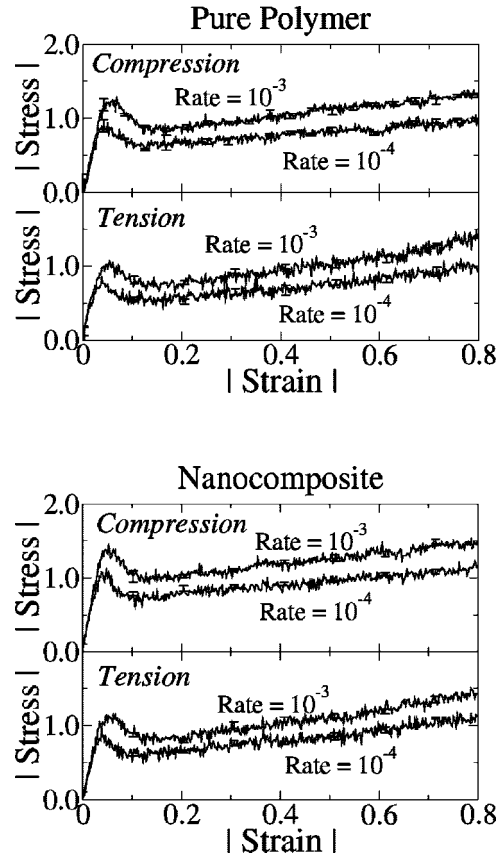

Figure 5. Stress−strain curves for both the pure polymer and the nanocomposite at two true strain rates in both tension and compression. The strain rates are indicated in each figure, and error bars are only shown on every 50 points for clarity.

regime. It is reassuring that these estimates of τ_{eff} using smaller time windows create a smooth curve joining the value of τ_{eff} from the undeformed materials to those estimated from the larger time windows; this observation gives us confidence that our time window approach does not significantly alter our results.

Similar to our analysis of the changes in U_{IS} during creep above, it is of interest to examine how constant-rate deformations alter the position of the materials on their PEL. Figure 7 plots U_{IS} against strain for both systems and all four constant strain rate deformations considered here. Prior to the yield point, U_{IS} increases rapidly; at the yield point, the rate of change of U_{IS} decreases, although U_{IS} continues to increase throughout the deformation. The addition of nanoparticles causes only a small increase in the absolute values of U_{IS}, and the changes in U_{IS} with deformation are approximately the same in the pure and the composite systems.

4. Discussion

4.1. Influence of Nanoparticles on Polymer Properties. The nanoparticles behave primarily as a stiffening agent in the model polymer considered in this work; this is evident from both the constant stress and constant strain rate deformation results presented above. For example, during creep with $\sigma = 0.59$ at a time of $t = 8000t_{LJ}$ the pure polymer has deformed to a strain of 0.41, while the nanocomposite has only deformed to 0.19. To achieve a similar strain of 0.40 in the same amount of time in the nanocomposite system, the applied stress must be increased to 0.65. Similarly, during constant strain rate deformations the nanoparticles increase the Young's modulus by ~50% in tension and 10% in compression, as discussed above. Additionally, the nanoparticles increase the yield stress for a given deformation rate, although the yield strain is approxi-

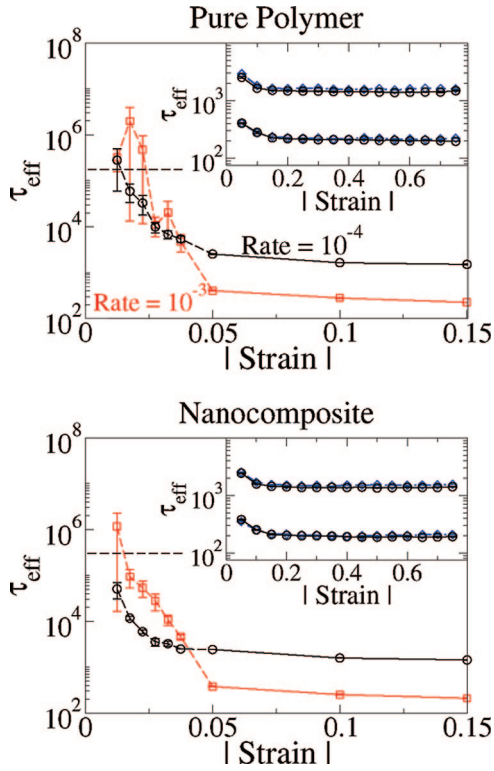

Figure 6. τ_{eff} as a function of strain for both the pure polymer and the nanocomposite. In both cases, the insets show τ_{eff} calculated with standard time window sizes versus strain for the entire endeformation (up to $|\epsilon| = 0.8$) for both tension (○) and compression (◇); the top pair of lines correspond to deformation at a rate of 10^{-4} while the bottom pair corresponds to a rate of 10^{-3}. The main figures enhance the changes in τ_{eff} at low values of strain for tensile deformation, and the points that lie along the dashed lines were determined using smaller time windows. The dashed horizontal line in the main figures represent τ_{eff} for an undeformed sample.

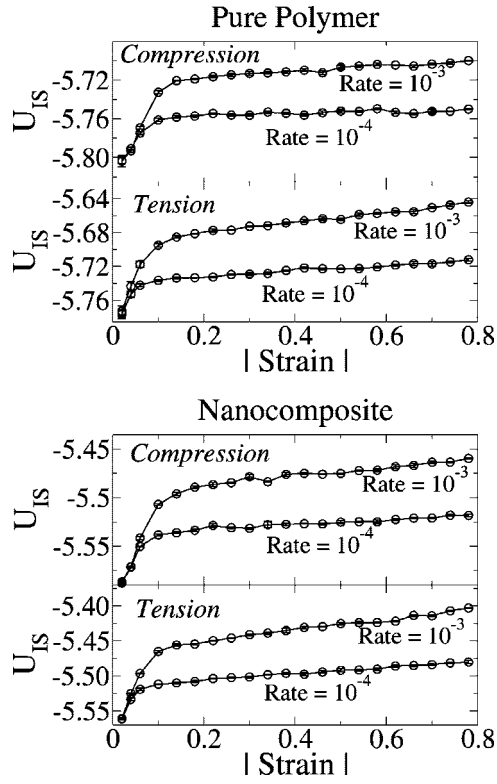

Figure 7. Inherent structure energy as a function of strain for the pure polymer and the nanocomposite during both tensile and compressive deformations at two different strain rates.

mately the same. Interestingly, for a given value of strain rate the mobility is approximately the same in both materials. This can be seen clearly from the constant strain rate results in Figure 6 and in Figure 9, discussed below. In addition to stiffening the polymer matrix, our nanoparticles also slightly swell the polymer chains; e.g., the radius of gyration increases from 11.2 ± 0.1 to 11.5 ± 0.04 up addition of the nanoparticles. Naturally, we expect that the effects of the nanoparticles to depend on the strength of the interaction between the polymer and the nanoparticles.[4,5] In this study, we have attempted to create a neutral nanoparticle akin to experiments using neutral nanoparticles such as cross-linked poly(styrene) spheres dispersed in a poly(styrene) matrix.[3]

It is of interest to examine whether the nanoparticles have any effect on the strain hardening modulus, G_R. We measure G_R by replotting the stress response from our constant strain rate deformations against $g(\lambda)$, the ideal rubber elasticity factor defined as $g(\lambda) = \lambda^2 - 1/\lambda$, where $\lambda = \exp(\epsilon)$ is the stretching ratio. Figure 8 shows the stress against $g(\lambda)$. After strain softening ($g(\lambda) > 0.5$), the stress becomes linear in $g(\lambda)$. This behavior is indicative of so-called Gaussian strain hardening, and the slope of the stress versus $g(\lambda)$ is the hardening modulus, G_R. We obtain G_R by fitting the region of the $\sigma - g(\lambda)$ curve where $0.5 \leq g(\lambda) \leq 2.0$; the results are summarized in Table 1. Generally speaking, the nanoparticles have a minimal effect on the hardening modulus for a given strain rate, and consistent with previous simulation studies on pure polymers,[28] we find that G_R increases with strain rate; interestingly, G_R is ~60% larger in compression than in tension at a constant strain rate, a trend inconsistent with the picture of strain hardening that arises from entropic rubber elasticity. A recent theory of Chen and Schweizer[27] postulates that strain hardening arises from anisotropic chain packing, which in turn leads to an increase in segmental relaxation times. This theory also predicts that G_R should be approximately twice as large in compression than in tension, consistent with our findings. The increase in segmental relaxation predicted by Chen and Schweizer at large deformation is not observed in our simulations (Figure 6); however, that discrepancy could arise from several sources, such as an interference between the β-relaxation and the α-relaxation that is difficult to resolve when we determine τ_{eff}.

For a given applied stress, Figure 3 demonstrates that the relaxation times in both systems can take a range of values covering nearly an order of magnitude. For example, in the pure polymer with an applied stress of 0.55, the first measurement of $\tau_{eff} \approx 20\,000$, yet later (at $t = 4500t_{LJ}$) $\tau_{eff} \approx 3000$. Such changes at constant stress and temperature are beyond the phenomena that can be captured by the Eyring model.[25] As described in the Introduction, the Eyring model does not consider phenomena such as flow and strain hardening, so it is not surprising that this model fails to capture the changes in the relaxation times. Complete details of the fit of our data to the Eyring model will be presented in a future publication.[31] Recent theoretical developments by Chen and Schweizer may be capable of describing the wide array of changes in τ_{eff} with deformation during both flow and strain hardening.[27]

4.2. Comparison of the Two Modes of Deformation. In our previous studies measuring the dynamics of a low molecular weight polymer during creep, we found a strong correlation between the instantaneous strain rate and the changes in τ_{eff}.[12,13] In those earlier studies, our polymer samples were smaller, and this led to appreciable variation in the results among different configurations. Here we are able to observe some of the more subtle details of the correlation between τ_{eff} and strain rate because the larger configurations in the present study provide a

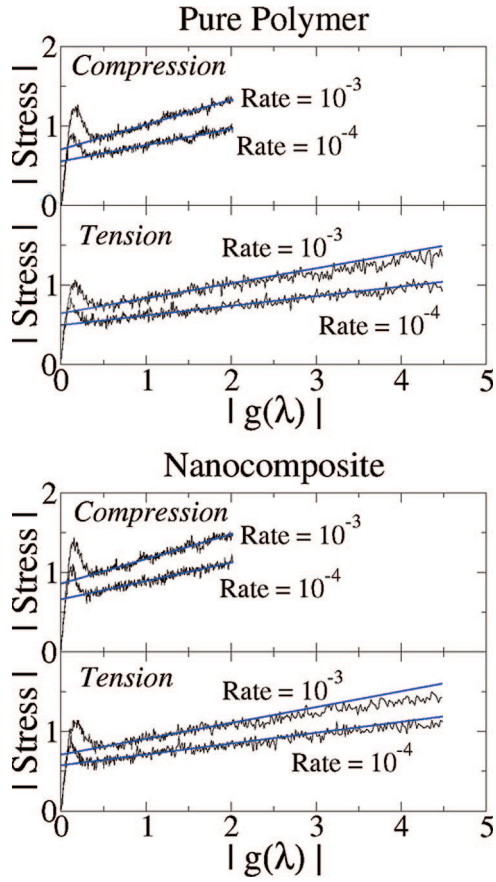

Figure 8. Stress plotted against $g(\lambda)$ for both the pure polymer and the nanocomposite at two true strain rates in both tension and compression. The strain rates are indicated in each figure, and the straight lines are linear fits to $0.5 \leq g(\lambda) \leq 2.0$.

Table 1. Values of G_R for the Pure Polymer and the Polymer Nanocomposite at Each Strain Rate and during Both Tension and Compression[a]

system	$\dot{\epsilon} = -10^{-3}$	$\dot{\epsilon} = -10^{-4}$	$\dot{\epsilon} = 10^{-3}$	$\dot{\epsilon} = 10^{-4}$
pure polymer	0.312	0.204	0.189	0.121
nanocomposite	0.310	0.230	0.199	0.137

[a] The uncertainty on each value of G_R is 0.01 or less.

higher resolution in τ_{eff}. Figure 9 shows τ_{eff} as a function of the instantaneous strain rate for both creep and constant strain rate simulations. Overall, the instantaneous strain rate provides a strong indicator of the changes in τ_{eff}, and τ_{eff} exhibits the largest decreases during periods of high strain rate. This is consistent with the "shear-thinning" behavior observed in our previous work.[13] However, there are systematic deviations from this trend. Early in the creep deformations (before the strain rate begins to decrease at $\epsilon \approx 0.20$), the estimates of τ_{eff} are systematically higher for a given strain rate (see the inset to Figure 9); similarly, τ_{eff} is larger in the elastic regime during the constant strain rate deformations, and the magnitude of the changes in τ_{eff} for $\epsilon \leq 0.20$ at a constant rate are approximately the same for constant strain rate and creep deformations. Taken together, these results indicate that a single mechanical variable (such as the strain rate) is not uniquely indicative of the dynamics. Note that Figure 9 does not include the estimates of τ_{eff} measured from the smaller time windows employed in Figure 6; including these points would generate a vertical column from the undeformed value of τ_{eff} to the postyield values of τ_{eff}, further emphasizing the fact that the strain rate does not uniquely dictate the dynamics.

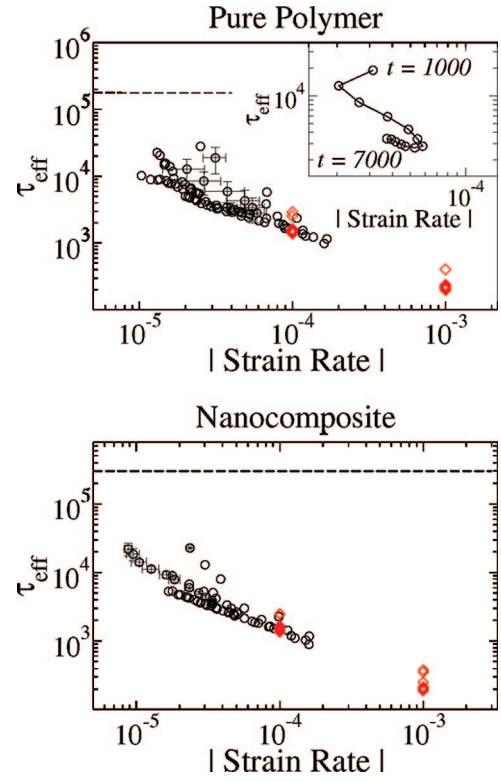

Figure 9. τ_{eff} plotted against the instantaneous strain rate measured during each time window for the creep deformations (○) of the pure polymer and the nanocomposite. Additionally, τ_{eff} as obtained during the constant strain rate deformations in both tension and compression is shown (◇). The dashed horizontal line represents τ_{eff} for the undeformed samples. The inset on the pure polymer figure shows all of the values of τ_{eff} and strain rate taken from one creep deformation with $\sigma = 0.59$, and the solid line connects the points in time. The first and last data points are indicated in the inset.

Interestingly, the nanoparticles appear to have a minimal effect on the value of τ_{eff} for a given value of strain rate. When deforming at a constant rate, the postyield values of τ_{eff} are approximately the same. This finding is also consistent with our results from creep deformations where, for a given value of strain rate, the estimates of τ_{eff} are approximately the same for the pure polymer and the nanocomposite. This leads us to the conclusion that, for the "standard" model considered in this work, the nanoparticles merely serve to enhance the mechanical properties.

In addition to the strain rate, our previous studies have shown that U_{IS} is strongly correlated to the mobility measured by τ_{eff} during creep.[13] We can test the robustness of this correlation by comparing the changes in U_{IS} with the changes in τ_{eff} during both constant-stress and constant strain rate deformations. Figure 10 shows U_{IS} as a function of τ_{eff} measured in the various time windows during both modes of deformation. For creep deformations, the data essentially collapse onto a single curve where $\log(\tau_{eff})$ decreases as U_{IS} increases. The trends are significantly different when we deform at a constant strain rate: τ_{eff} changes by a much smaller amount, and it is almost independent of U_{IS}. The values of τ_{eff} obtained from either tensile or compressive constant strain rate deformations have approximately the same value, but U_{IS} is significantly different. These results provide a striking evidence of the fundamental differences between the two deformation mechanisms considered here, although such differences could be due to the different strains achieved under creep or constant rate. All of the constant-rate deformations proceeded until the strain was $|\epsilon| = 0.8$, while the largest strains reached under creep were only $\epsilon \approx 0.55$.

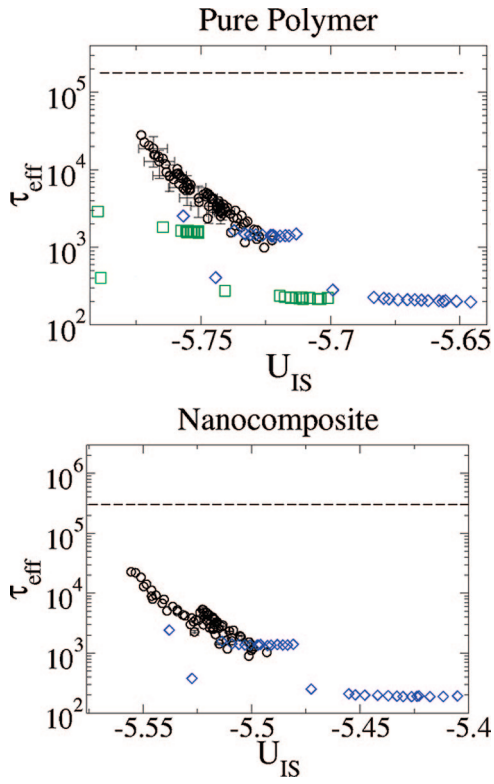

Figure 10. τ_{eff} plotted against U_{IS} for both systems, where τ_{eff} is obtained during the creep deformations (○), tensile deformations at a constant strain rate (◇), and compressive deformations at a constant rate (□).

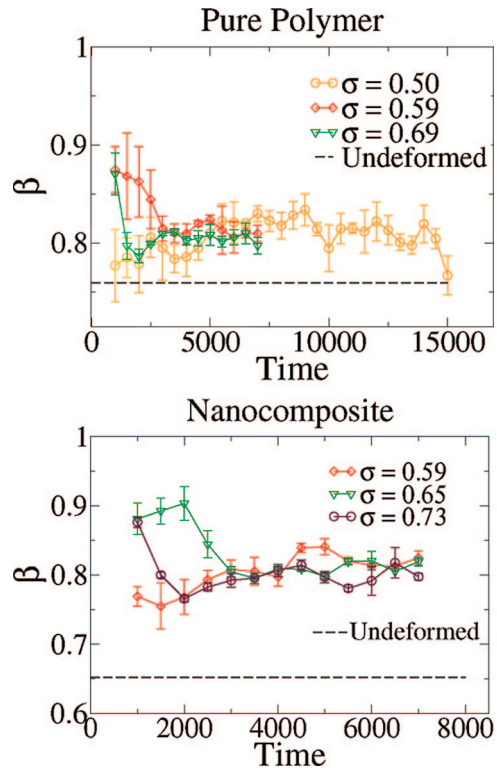

Figure 11. KWW stretching exponent β as a function of time during the creep deformations for three of the applied stresses for both the pure polymer and the nanocomposite.

4.3. Dynamic Heterogeneity. When we fit $C_b(t)$ in each time window we obtain the KWW stretching exponent β along with τ_{eff}. The exponent β can be qualitatively correlated with the fragility of glass-forming materials[39,40] and is often interpreted as a measure of the dynamic heterogeneity that arises in supercooled liquids. Typically β increases toward unity as the temperature is increased from T_g to T_A, the temperature where the dynamic properties (e.g., α-relaxation time and the diffusivity) exhibit an Arrhenius temperature dependence. Experiments indicate that β should increase toward unity as τ_{eff} decreases, and it is of interest to examine whether our simulations can reproduce this trend. The changes in β during creep deformations are shown in Figure 11, and the changes during constant rate deformations are in given in Figure 12. In all cases, β is higher during deformation than at rest, indicating that deformation leads to a decrease in the dynamic heterogeneity and a homogeneization of the material. During creep deformations, β is only weakly correlated with the instantaneous strain rate, and no strong trend in relation to the mechanical features of Figure 1 can be discerned. For the constant strain rate deformations, we see in Figure 12 that there is not one value of β for a given strain rate, even though τ_{eff} is approximately constant after yield (see Figure 6) for a given strain rate. Initially, β begins at a value much larger than its value at rest and decreases during the elastic regime. The rate of decrease then slows down for all applied strain rates before β continues to slowly decrease as the deformation proceeds. This complex dependence of β on the deformation protocol is still under investigation.

While the value of β obtained from fitting to the KWW equation provides some insight into the dynamic heterogeneity present in each system, difficulties arise due to the uncertainty of our calculations as well as the limited range that β is expected to cover in simulations. We do not expect β to be larger than unity, and our undeformed value of β is 0.76 ± 0.05. We therefore turn to other measures of the dynamic heterogeneity by calculating the self-part of the van Hove correlation function, $G_S(r,\delta t)$. $G_S(r,\delta t)$ measures the probability that a particle has moved a distance r after time δt, provided that it was at the origin when $\delta t = 0$. For values of δt where the motion of a material is diffusive, $G_S(r,\delta t)$ can be described by a Gaussian. For supercooled liquids on intermediate time scales (before diffusive motion sets in), $G_S(r,\delta t)$ exhibits significant departures from Gaussian behavior.[41,42] For simplicity, we only focus on $G_S(r,\delta t)$ as calculated from the constant strain rate deformations.

Figure 13 shows how $G_S(r,\delta t)$ changes during our constant strain rate deformations in both systems during the elastic regime, strain softening, and strain hardening. The strain softening and hardening regimes both have approximately the same distribution of particle displacements, and this distribution is similar to a Gaussian distribution with an enhanced "shoulder" for large r. During the elastic regime, the overall distribution of displacements is shifted to smaller r, and the shoulder on the distribution is more pronounced; while most of the particles have only been displaced by a small amount, there is a clear subset of particles that have moved approximately twice as far. These particles are likely involved in the so-called "plastic events" that occur prior to yield in many glass-forming systems.[43−46] There are no qualitative differences between the pure polymer and the nanocomposite. This is expected given the similarity in the values of τ_{eff} obtained for the two systems when we deform at a constant strain rate.

5. Summary

In this study, we have performed extensive Monte Carlo and nonequilibrium molecular dynamics simulations of a glassy polymer and a polymer nanocomposite, extending our previous work in several key areas. We have examined the creep response of these materials and the corresponding stress−strain curves during both compression and tensile deformations. It is found that nanoparticles stiffen the polymer, leading to higher elastic moduli and a suppression of the creep response. Beyond those

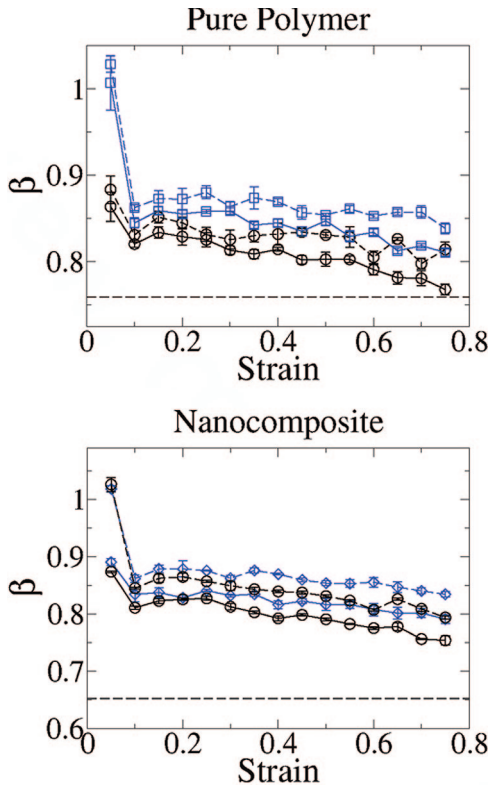

Figure 12. KWW stretching exponent β as a function of strain for deformation at a constant strain rate for both the pure polymer and nanocomposite systems. The solid lines correspond to deformation at a strain rate of 10^{-4}, and the dashed lines are deformed at a strain rate of 10^{-3} for both tension (black lines with ○) and compression (blue lines with ◇).

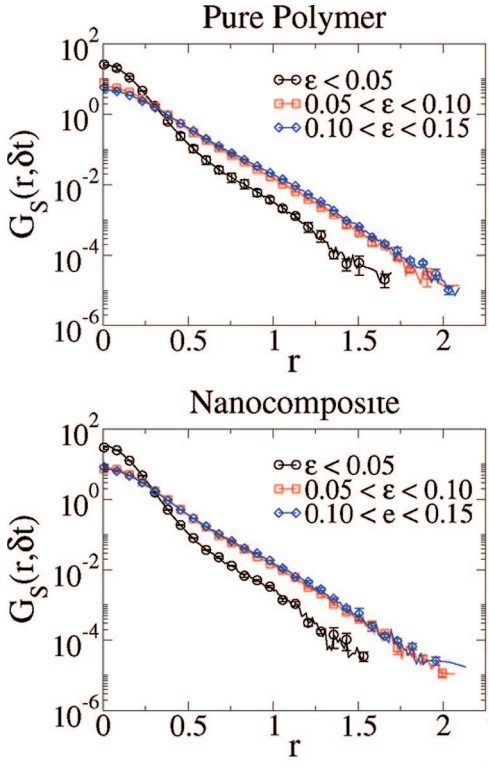

Figure 13. Self-part of the van Hove correlation function, $G_S(r,\delta t)$, for the pure polymer and the polymer nanocomposite at three points during the constant rate deformations. δt is chosen such that it spans a strain of approximately $\epsilon = 0.05$ in each case.

effects, for the standard composite model adopted in this work, the composite and the polymer behave in surprisingly similar manners. For both the pure polymer and the composite the deformation imparts a significant (over 2 orders of magnitude in some cases) change to the relaxation times. In general, the relaxation time is correlated with the instantaneous strain rate, although there are systematic deviations from this trend. No single mechanical variable is capable of capturing the changes of the relaxation time with deformation. Additionally, we have explored the extent to which a material's position on its potential energy landscape can indicate the dynamics and found that this correlation breaks down during deformation at a constant strain rate.

Acknowledgment. We acknowledge the National Science Foundation for funding through the MRSEC on nanostructured interfaces at the University of Wisconsin and the NIRT program (NIRT Grant CTS-0506840). We are grateful for valuable discussions and suggestions from M. D. Ediger, Hau-Nan Lee, K. S. Schweizer, and J. Caruthers.

References and Notes

(1) Zhang, Q.; Archer, L. A. *Langmuir* **2002**, *18*, 10435.
(2) Sternstein, S. S.; Zhu, A.-J. *Macromolecules* **2002**, *35*, 7262.
(3) Mackay, M. E.; Dao, T. T.; Tuteja, A.; Ho, D. L.; Horn, B. V.; Kim, H.-C.; Hawker, C. J. *Nat. Mater.* **2003**, *2*, 762.
(4) Papakonstantopoulos, G. J.; Yoshimoto, K.; Doxastakis, M.; Nealey, P. F.; de Pablo, J. J. *Phys. Rev. E* **2005**, *72*, 031801.
(5) Papakonstantopoulos, G. J.; Doxastakis, M.; Nealey, P. F.; Barrat, J.-L.; de Pablo, J. J. *Phys. Rev. E* **2007**, *75*, 031803.
(6) Schadler, L. *Nat. Mater.* **2007**, *6*, 257.
(7) Kopesky, E. T.; McKinley, G. H.; Cohen, R. E. *Polymer* **2006**, *47*, 299.
(8) Kopesky, E. T.; Haddad, T. S.; McKinley, G. H.; Cohen, R. E. *Polymer* **2005**, *46*, 4743.
(9) Loo, L.; Cohen, R.; Gleason, K. *Science* **2000**, *288*, 116.
(10) Lee, H.-N.; Pang, K.; Swallen, S. F.; Ediger, M. D. *J. Chem. Phys.* **2008**, *128*, 134902.
(11) Chen, K.; Schweizer, K. S. *Eur. Phys. Lett.* **2007**, *79*, 26006.
(12) Riggleman, R. A.; Lee, H.-N.; Ediger, M. D.; de Pablo, J. J. *Phys. Rev. Lett.* **2007**, *99*, 215501.
(13) Riggleman, R. A.; Schweizer, K. S.; de Pablo, J. J. *Macromolecules* **2008**, *41*, 4969.
(14) Lacks, D. J. *Phys. Rev. Lett.* **2001**, *87*, 225502.
(15) Lacks, D. J.; Osborne, M. J. *Phys. Rev. Lett.* **2004**, *93*, 255501.
(16) Frey, M. M.; Lacks, D. J. *J. Chem. Phys.* **2000**, *112*, 2909.
(17) Nandagopal, M.; Utz, M. *J. Chem. Phys.* **2003**, *118*, 8373.
(18) Berthier, L.; Barrat, J.-L. *J. Chem. Phys.* **2002**, *116*, 6228.
(19) Varnik, F. *J. Chem. Phys.* **2006**, *125*, 164514.
(20) Utz, M.; Debenedetti, P. G.; Stillinger, F. H. *Phys. Rev. Lett.* **2000**, *84*, 1471.
(21) Capaldi, F. M.; Boyce, M. C.; Rutledge, G. C. *Phys. Rev. Lett.* **2002**, *89*, 175505.
(22) Lyulin, A. V.; Balabaev, N. K.; Mazo, M. A.; Michels, M. A. J. *Macromolecules* **2004**, *37*, 8785.
(23) Lyulin, A. V.; Vorselaars, B.; Mazo, M. A.; Balabaev, N. K.; Michels, M. A. J. *Europhys. Lett.* **2005**, *71*, 618.
(24) Warren, M.; Rottler, J. *Phys. Rev. E* **2007**, *76*, 031802.
(25) Eyring, H. *J. Chem. Phys.* **1936**, *4*, 283.
(26) Lee, H.-N.; Pang, K.; Swallen, S. F.; Ediger, M. D. *Science* **2009**, *323*, 231.
(27) Chen, K.; Schweizer, K. S. *Phys. Rev. Lett.* **2009**, *102*, 038301.
(28) Hoy, R. S.; Robbins, M. O. *J. Polym. Sci., Part B: Polym. Phys.* **2006**, *44*, 3487.
(29) Hoy, R. S.; Robbins, M. O. *Phys. Rev. Lett.* **2007**, *99*, 117801.
(30) Hoy, R. S.; Robbins, M. O. *Phys. Rev. E* **2008**, *77*, 031801.
(31) Lee, H.-N.; Riggleman, R. A.; Ediger, M. D.; de Pablo, J. J. *Macromolecules*, submitted.
(32) Riggleman, R. A.; Douglas, J. F.; de Pablo, J. J. *J. Chem. Phys.* **2007**, *126*, 234903.
(33) Jain, T. S.; de Pablo, J. J. *J. Chem. Phys.* **2004**, *120*, 9371.
(34) Banaszak, B. J.; de Pablo, J. J. *J. Chem. Phys.* **2003**, *119*, 2456.
(35) Karayiannis, N. C.; Mavrantzas, V. G.; Theodorou, D. N. *Phys. Rev. Lett.* **2002**, *88*, 105503.
(36) Plimpton, S. J. *J. Comput. Phys.* **1995**, *117*, 1.
(37) Riggleman, R. A.; Yoshimoto, K.; Douglas, J. F.; de Pablo, J. *J. Phys. Rev. Lett.* **2006**, *97*, 045502.

(38) Bennemann, C.; Paul, W.; Baschnagel, J.; Binder, K. *J. Phys.: Condens. Matter* **1999**, *11*, 2179.
(39) Bohmer, R.; Ngai, K. L.; Angell, C. A.; Plazek, D. J. *J. Chem. Phys.* **1993**, *99*, 4201.
(40) Abraham, S. E.; Bhattacharrya, S. M.; Bagchi, B. *Phys. Rev. Lett.* **2008**, *100*, 167801.
(41) Kob, W.; Donati, C.; Plimpton, S. J.; Poole, P. H.; Glotzer, S. C. *Phys. Rev. Lett.* **1997**, *79*, 2827–2830.
(42) Chaudhuri, P.; Berthier, L.; Kob, W. *Phys. Rev. Lett.* **2007**, *99*, 060604.
(43) Papakonstantopoulos, G. J.; Riggleman, R. A.; Barrat, J.-L.; de Pablo, J. J. *Phys. Rev. E* **2008**, *77*, 041502.
(44) Léonforte, F.; Tanguy, A.; Wittmer, J.; Barrat, J.-L. *Phys. Rev. Lett.* **2006**, *97*, 055501.
(45) Argon, A. S.; Bulatov, V. V.; Mott, P. H.; Suter, U. W. *J. Rheol.* **1995**, *39*, 377.
(46) Falk, M. L.; Langer, J. S. *Phys. Rev. E* **1998**, *57*, 7192.

MA802865N